Materials Science & Engineering B 228 (2018) 91–95

Contents lists available at ScienceDirect

Materials Science & Engineering B

journal homepage: www.elsevier.com/locate/mseb

Single step chemical growth of ZnMgS nanorod thin film and its DFT study

Avinash S. Dive[a], Ketan P. Gattu[b], Nanasaheb P. Huse[a], Devesh R. Upadhayay[c], D.M. Phase[d], Ramphal B. Sharma[a,b,*]

[a] Thin Film and Nanotechnology Laboratory, Department of Physics, Dr. Babasaheb Ambedkar Marathwada University, Aurangabad 431004, MS, India
[b] Department of Nanotechnology, Dr. Babasaheb Ambedkar Marathwada University, Aurangabad 431004, MS, India
[c] SRM University, SRM Nagar, Kancheepuram District, Kattankulathur, Tamil Nadu 603 203, India
[d] UGC DAE Consortium for Scientific Research, Indore 452001, MP, India

ARTICLE INFO

Keywords:
Nanorods
ZnMgS
Chemical bath deposition
DFT

ABSTRACT

Herein, ZnMgS nanorod (NR) thin film has been grown by facile single step chemical bath deposition technique. Initially, vertically aligned ZnMgS NR having ~3 μm length and diameter of ~200 nm were deposited on commercial glass substrate. The morphology characterizations of this nanorod thin film were observed by FE-SEM and TEM. The randomly oriented hexagonal type nanorods were grown on the glass surface. The strong and highly intense (0 0 2) peak in the XRD pattern along with the calculated low compressive strain indicates vertical growth of high-quality crystalline ZnMgS nanorods. The films showed a direct band transition at ~3.62 eV. The photosensing properties of NR thin film of ZnMgS showed an excellent photoresponsivity of 34.6 μA/Watt and photosensitivity 99% respectively under illumination of 100 W/cm^2 at a bias voltage 5 V. The obtained experimental results were found to be consistent with theoretical results obtained using DFT.

1. Introduction

Wide-band-gap semiconductors, mainly those with wurtzite structure, are of interest for a range of technological applications [1]. For example, II-VI system such as ZnS or ZnO nanostructure has widely been utilized in optoelectronic devices such as light-emitting diodes (LED), photosensor/photodetectors, gas sensors, electroluminescence, flat panel displays and now as a window layer in a solar cell, etc. [2]. Recently, ternary alloy ZnMgS have been seeking the attention of many researchers as alternative device materials due to their outstanding properties. Among these large excitation binding, energy and wide bandgap are important for opto-electronic applications etc. [3,4]. The control over the shape of the nanostructure is another important factor for the development of such materials, the elongated one-dimensional (1-D) morphology such as nanorods, nanowires, nanofibers has thus been focused by many researchers for a wide range of applications. Nanorods, nanotubes are important and popular 1-D nanostructures [5]. Nanorods are short as well as stiff with prevalent circular cross-sections, but can often have hexagonal cross-sections [6]. There are a large number of reports available on the chemical and physical synthesis of 1-D nanostructures, such as physical vapor deposition [7], chemical bath deposition [8], hydrothermal synthesis [9,10], solvothermal approach [11,12] radio frequency magnetron sputtering technique [12], etc. Considering the advantages of chemical synthesis over physical methods and with an aim of mixing materials/sources at atomic level [13] so that the materials are close enough to form thermodynamic equilibrium, we have chosen chemical synthesis in our present work. According to the phase diagram, the solubility of Mg in ZnS at normal condition is of eutectic type [14]. There are few reports available on the extensive solubility of the Mg in zincite is up to 33 mol % [15]. Furthermore, the solubility depends upon the experimental condition such as temperature and pressure. ZnMgS exhibit the stable wurtzite (WZ) structure below the 4 mol% Mg. Mg^{2+} has an ionic radius of 0.57 Å which is very close to Zn^{2+} 0.60 Å, therefore it can easily dope with Mg^{2+} [16]. Pure MgS has a higher band gap as compared to ZnS because the incorporation Mg will increase the band gap [17]. Mg alloying in ZnS modulates the fundamental band gap [18], which allows its use as a barrier material in the quantum well structure for optoelectronic devices [3,4,19]. ZnMgS alloy is reported to be synthesized by various physical techniques such as molecular beam epitaxy [4], pulsed laser deposition [20] etc. As per our up to date literature survey there are very few reports available on the synthesis of ZnMgS thin films by the chemical approach. Further, to understand the behaviour of the materials, it is essential to study both their crystal structure and electronic structures.

Thus in the present manuscript, we have focused on the synthesis, characterization, and correlation of structural and optical properties of pure ZnMgS 1-D nanorod thin films with theoretical study. In this

* Corresponding author at: Thin Film and Nanotechnology Laboratory, Department of Physics, Dr. Babasaheb Ambedkar Marathwada University, Aurangabad 431004, MS, India.
E-mail address: rps.phy@gmail.com (R.B. Sharma).

https://doi.org/10.1016/j.mseb.2017.11.018
Received 21 July 2017; Received in revised form 4 November 2017; Accepted 20 November 2017
Available online 22 November 2017
0921-5107/

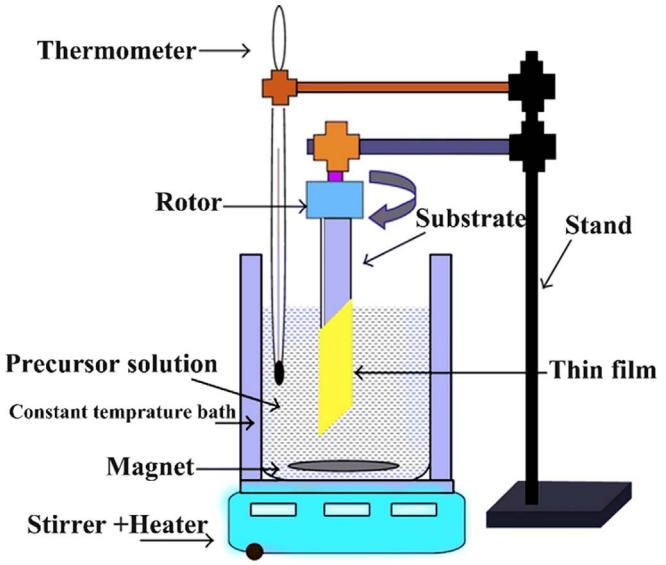

Fig. 1. (a) Schematic of a chemical bath deposition.

ternary alloy, Mg plays a role of donor atom into the host lattice, which is expected to result in promising optical properties that can be investigated experimentally as well as theoretically. The ZnMgS 1-D nanorods have been grown on the amorphous glass substrate using single-step chemical approach. Also, we report here ZnMgS 1-D NR thin film grown by very short deposition time of 1 h. and relatively low bath temperature i.e. 65 °C. ZnMgS 1-D NR thin film was further characterized for its structural, morphological, optical, electrical and electronic properties.

2. Materials and methods

2.1. Synthesis of ZnMgS 1-D nanorods

Fig. 1 shows a schematic for the synthesis of ZnMgS NR thin film using single-step chemical bath deposition technique on a commercial glass (silica) slides. Initially, the glass slides were kept in chromic acid for 4 h. at ~100 °C and then subsequently washed with deionized water (DI) and laboline detergent. This cleaning of the substrate is an important to step in the deposition process to obtain uniform thin film and achieve better adhesion and stoichiometry.

All the chemicals used for the deposition of ZnMgS NR were analytical reagent (AR) grade and were used without further purification. In the typical synthesis procedure, an aqueous solution of zinc nitrate hexahydrate [$Zn(NO_3)_2{\cdot}6H_2O$: 0.08 M], magnesium nitrate hexahydrate [$Mg(NO_3)_2{\cdot}6H_2O$: 0.02 M] and thiourea [H_2NCSNH_2: 0.1 M] were dissolved in 30 ml DI water with constant stirring (each for 20 min) in different beakers. After dissolving, the sources in respective beakers 2 drops of triethanolamine (TEA) were added in zinc source solution and immediately the precipitate forms in a beaker. Afterwards, ammonia was added dropwise with constant stirring till solution gets clear. The pH of the final clear salt solution was ~11. Finally, the source of the magnesium and sulphur were added in zinc solution slowly with constant stirring. The obtained solution was placed in a hot water bath maintained at a temperature of ~65 °C. The pre-cleaned glass substrates were immersed vertically in the beaker for 60 min. The obtained films were yellowish white in colour with uniform deposition over the entire surface of the substrate. The films were washed with deionized water to remove weakly bonded atoms on the surface and dried subsequently.

2.2. Characterization of ZnMgS 1-D nanorods

The as-synthesized ZnMgS NR thin film were characterized by different characterization techniques. The crystal structure and phase of the as-grown ZnMgS NR thin film were confirmed by Bruker AXS, Germany (D8 Advanced) X-ray Diffractometer. A scanning rate of 0.05 s^{-1} was applied to record the patterns in scanning range 20–80°(2θ) using $CuK\alpha_1$ radiation with wavelength 1.5406 Å. Transmission electron microscopy (TEM) measurements were carried out at an accelerating voltage of 200 kV, and selected-area electron diffraction (SAED) patterns were obtained using Tecnai G2 20 at an acceleration voltage of 200 kV. The compositional and morphological analysis was carried out by energy dispersive X-ray (EDAX) attached to field emission scanning electron microscopy (FE-SEM) instrument MIRA II LMH from TESCAN with an accelerating voltage of 5 and 30 kV. The optical properties of the films, the absorbance spectra were recorded in 300–1100 nm range using UV–Vis spectrophotometer Perkin Elmer Lambda-25. The I-V characteristics were obtained by illuminating the of solar simulator lamp as a light source for acquiring the data on Keithley 2400 measurement setup interfaced with a computer. The optimized and calculated results are reported in the manuscript.

2.3. Computational details

Structural, electronic, and optical properties of ZnMgS are studied by solving the Kohn–Sham equations using Medea-VASP package. A 2 × 2 × 2 supercells were built with the wurtzite ZnMgS unit cell with $P6_3mc$ as the space group. To study, the Magnesium (Mg) atom incorporated into the ZnS system, one Zinc (Zn) atom was replaced with the Magnesium (Mg) atom in the supercell. The exchange and correlation energy are described by generalized gradient approximation (GGA) for the structural properties and Perdew-Burke-Ernzerhof (PBE) potential for the electron-electron correlation effect [21,22]. The optimized supercell for the DFT calculations formed as $MgZn_{15}S_{16}$. The residual force of 0.01 eV/Å for varying internal position of atoms was used to attain the minimum energy state as well as 400 eV was set as the cutoff kinetic energy [23]. A 2 × 2 × 2 K-mesh was used which correspond to spacing less than 0.5 Å in reciprocal space. Methfessel-Paxton type of smearing was used with smearing width of 0.2 eV. Real space projection operator was used as the system contains a large number of atoms.

3. Result and discussion

3.1. XRD analysis

XRD analysis is important characterization tool towards understanding the structural properties of a material. Fig. 2 shows the typical XRD pattern of as-grown ZnMgS NR thin film which clearly indicates the formation of pure ZnMgS composition having wurtzite hexagonal crystal structure (JCPDS # 37-1180). The diffraction peaks observed at 29.22° (1 1 1), 31.78° (1 0 0), 34.42° (0 0 2), 36.26° (1 0 1), 47.54° (2 2 0) 56.6° (3 1 1), 62.88° (2 0 2), 68° (1 1 2), 69° (2 0 1) and 72.6° (0 0 4) corresponds to wurtzite structure of ZnMgS.

The strong and sharp diffraction peak at 34.42° with very high intensity confirms the direction of NR along normal to the surface of the sample [24], this is also confirmed from FE-SEM micrographs and its cross-section view. Kai Huang et al. reported that the pure ZnO having a polycrystalline nature, while Mg-ZnO (2–8 atomic%) thin films show a preferential c-axis orientation, additionally shows a phase separation after 8 at.% of Mg content [25]. Herein our reports we get better crystalline quality as well as uniform deposition. Lattice parameters for wurtzite phase were calculated with help of the following standard Eq. (1), the average crystallite size was calculated by the following Scherrer formula Eq. (2) and the strain of the ZnMgS NR thin films calculated by

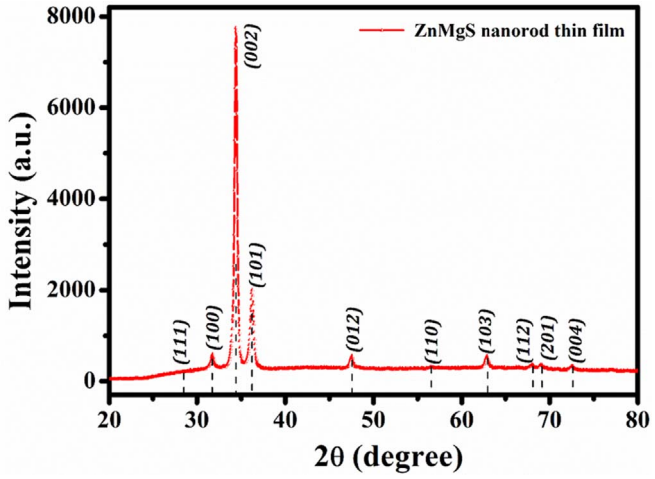

Fig. 2. X-ray diffraction patterns of ZnMgS NR thin films.

following Eq. (3) [26,27],

$$\frac{1}{d^2} = \frac{4}{3}\left(\frac{h^2 + hk + k^2}{a^2}\right) + \frac{l^2}{c^2} \quad (1)$$

$$D = \frac{0.9\lambda}{\beta cos\theta} \quad (2)$$

$$strain = \frac{\beta cos\theta}{4} \quad (3)$$

The calculated parameters such as strain, average crystallite size, and lattice parameters are shown in Table 1. The obtained results from XRD were well supported with the TEM and SAED results.

3.2. Surface morphological analysis

FE-SEM is a convenient and versatile method to study and analyze the surface morphology of thin films. Typical FE-SEM micrographs of the ZnMgS NRs grown on the amorphous glass substrate are shown in Fig. 3(a), (b). The image shows the formation of a uniform layer of 1-D NR. Which can be further confirmed by the later representations of electron microscopy (TEM) images Fig. 3(c) shows the EDX spectrum of the grown ZnMgS NR thin film, showing peaks for both Zn, Mg, S and O atoms with approximately similar atomic percentage (50: 15: 25: 10) respectively, this confirms the atomic composition of prepared ZnMgS NR thin film to be nearly stoichiometric within the limits of experimental error. The presence of ~15% oxide phase which may be due to DI water used as a solvent in the reaction [28].

3.3. TEM analysis

TEM images were obtained to get the detailed information regarding the physical structure of the grown ZnMgS NR thin film. Although, TEM images showing in the plane and focused view of the ZnMgS NR thin film were obtained showed in Fig. 3(d) and (e). The average diameter of the NR is ~200 nm and the average length is ~3 μm. The average crystallite size from TEM image of was ~30 nm, this is in good agreement with the XRD results. Here we can conclude, a suitable amount and optimized concentration of zinc, magnesium and sulphur solution in a reaction will be in the favour of nucleation of WZ ZnMgS NR's because the NRs grew towards [0 0 2] plane. The selected area electron diffraction (SAED) pattern obtained from the sample is presented in Fig. 3(f). The SAED pattern shows discrete spot pattern which is the characteristic of nanorods, which confirms the film containing 1-D NR's. The spots in the SAED pattern further indexed for the WZ structure.

Table 1
Structural parameters of ZnMgS NR thin film estimated from XRD data.

Sample	Lattice Parameters a (Å)	c (Å)	c/a ratio	Strain	Average crystallite Size (nm)	# JCPDS
ZnMgS NR thin film	3.70	5.20	1.43	0.0044	23	37-1180

3.4. Optical study

The UV–vis absorption spectra obtained for ZnMgS NR thin film deposited on a glass substrate is shown in Fig. 4(a). In this study, the absorbance of samples was measured as a function of wavelength in the range of 200–900 nm. The absorbance is estimated to depend on some factors such as band gap, surface roughness, oxygen deficiency and impurity centers [15,29]. The absorbance spectra show UV cut off at around 350–380 nm, due to the photoexcitation of electrons from valence to conduction band. The bandgap of the as-grown ZnMgS NR thin film was calculated by extrapolating the plot of $(\alpha h\nu)^2$ vs $h\nu$ using the Tauc's relation [30].

$$(\alpha h\nu) = A(h\nu - Eg)^n \quad (4)$$

where A is a constant and n is equal to 1/2 for direct bandgap semiconductors [31]. The plot of $(\alpha h\nu)^2$ vs. $h\nu$ is shown in Fig. 4(b) (Inset). The bandgap obtained for the ZnMgS NR thin film is ~3.62 eV. The calculated result showed that the band gap of ZnMgS NR thin film was ~3.62 eV, larger than pure bulk ZnS. This may be attributed to the fact that new defects are introduced after Mg atoms placed in Zn lattice site due to the electronegativity and ionic radius difference [32]. The obtained bandgap, in this case, matches well with the reported values of ZnMgS. Normally in n-type semiconductor, the Fermi level is inside the conduction band while the Mg contributes more electrons due to lower electron affinity. Which may be positioned at higher Fermi level for ZnMgS thin film which may lead to a blue shift [18]. This result is also reliable with theoretical and practical results. Such a kind of broad and fine band gap properties of ternary alloy ZnMgS NR thin film have potential applications in optoelectronic devices.

3.5. Electrical study

To study the transport properties ZnMgS NR thin film, we measured the current density-voltage (J–V) characteristics at room temperature in dark and in presence of light of solar simulator lamp with an intensity of 100 W/cm^2. Fig. 5 shows the J-V plots of ZnMgS NR thin films for 5 V applied bias. 1 × 1 cm film was used to study the photosensing phenomenon, a silver paste was used to make electrical contacts with the film as per shown the schematic in Fig. 1. The current is proportional to the applied voltage, which means ohmic behaviour showed by the NR thin film [33,34]. A considerable change in current under illumination of 100 W/cm^2 was observed which is associated with the generation of free electron-hole pairs in the conduction and valence band because of the incident photons. Due to incident photon energy breaks some covalent bonds which increase charge carrier concentration both in the valence band and conduction band by creating free electron and hole respectively. The calculated resistance of the ZnMgS NR thin film in dark and under illumination was found to be $1.44 \times 10^8\ \Omega$ and $1.43 \times 10^6\ \Omega$ respectively.

The photosensitivity (S) and photoresponsivity (R) were calculated and found to be ~99% and ~34.6 μA/Watt respectively by using the Eqs. (5), (6) [26].

$$S\ (\%) = \frac{R_d - R_l}{R_d} \times 100 \quad (5)$$

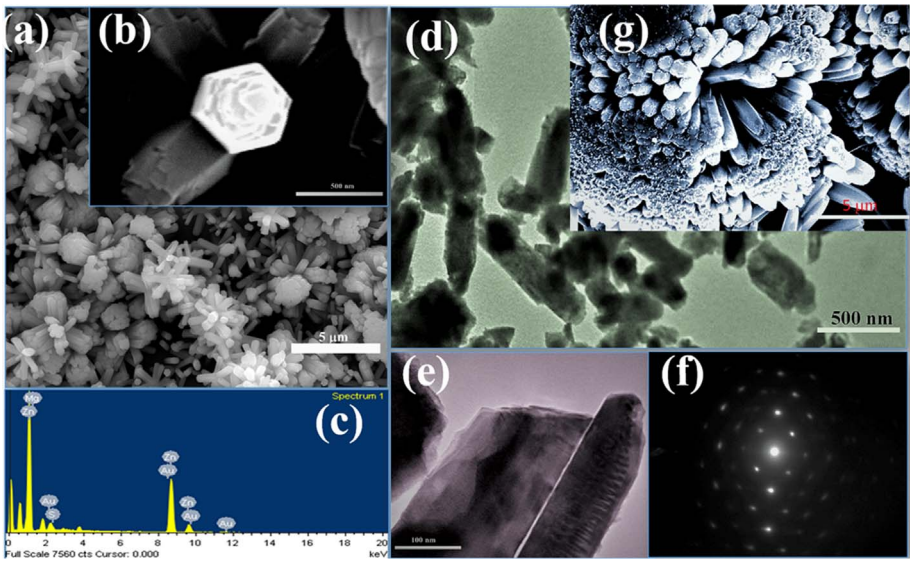

Fig. 3. (a) Top view of FE-SEM image of ZnMgS NR thin film (b) magnifying view of single nanorod (c) EDAX spectra of ZnMgS NR thin film, (d) and (e) Plane view of TEM images of ZnMgS NR thin film (f) selective area diffraction pattern (g) cross-section FE-SEM view of ZnMgS NR thin film.

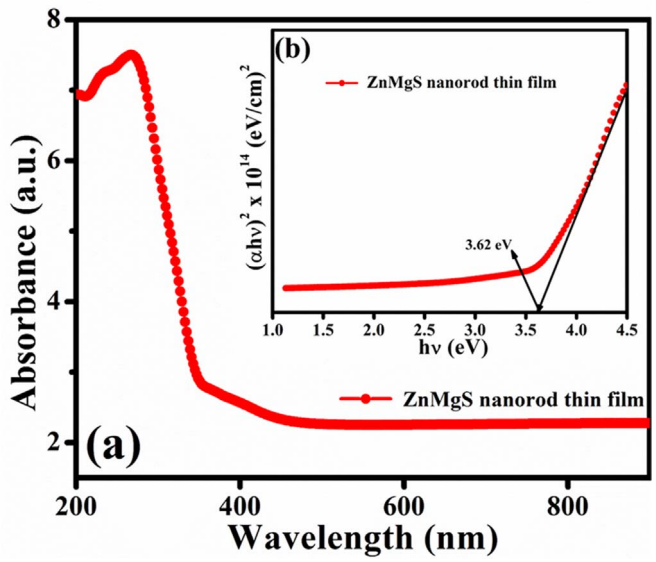

Fig. 4. (a) UV–Vis spectra of ZnMgS NR thin films (b) bandgap of ZnMgS NR thin film.

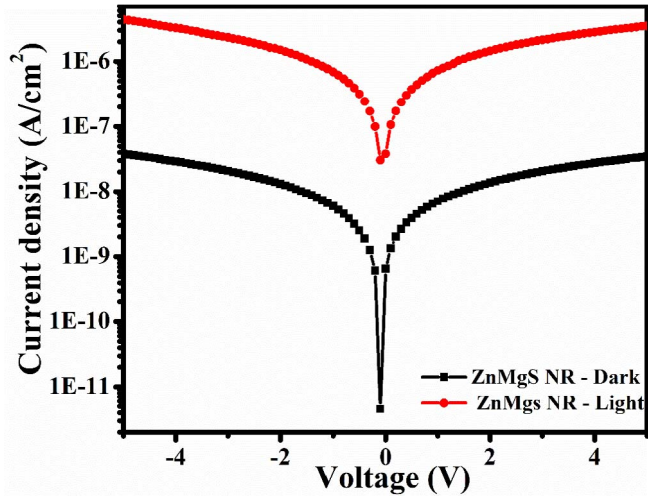

Fig. 5. J-V plots of ZnMgS NR thin film under dark and under illumination of 100 Watt/cm^2.

$$R = \frac{I_p - I_d}{SP_i} \tag{6}$$

3.6. Electronic structure investigation

In order to confirm the experimental results of ZnMgS NR thin film, theoretical band gap, total, partial and summed density of states have been studied by using Generalized Gradient Approximation (GGA) of the Density Functional Theory (DFT) with the help of Vienna Ab initio Simulation Package (VASP). The structural optimization was performed for wurtzite ZnMgS and the lattice parameters of the optimized structure where a = 3.83 Å, c = 6.27 Å. Further, the band structure was calculated for the optimized structure and shown in Fig. 6(a). From the theoretical band structure, ZnMgS exhibit the direct band semiconductors with an energy band gap of 1.53 eV. The band profile of the wurtzite structure shows that the conduction band minima and the valence band maxima are located at Γ point of the first Brillion zone, hence the material is a direct bandgap semiconductor shown in Fig. 6.

The semiconducting nature of the film was also confirmed in electrical studies which are correlated here. Khan et al. reported the theoretical results on rock-salt ZnMgS having indirect band gap and the indirect band gap materials are optically inactive due to their phonon addition in between electron and photon [35,36]. Therefore, we could state that the direct band gap compounds are dominant in the field of optoelectronics in comparison with indirect band gap materials [37]. From this, the WZ structure of ZnMgS is needed to be maintained for its efficient use in the optoelectronic device application. The bandgap results reported here are close to the previous reports of wurtzite -ZnMgS calculated using WC-GGA approximation.

It is a well-known problem in the theoretical study, that (localized density approximation) LDA and GGA calculations locate at the Zn-3d band incorrectly, which is close to the top of the valence band, and its strong hybridization with the O-2p misrepresents the band dispersion [38,39]. Hence, the reduction in the band gap energy as compared to the experimental band gap energy values. Fig. 6(b) shows schematic representatives of atom-resolved total and partial density of states (DOS) of ZnMgS. The dominance in the density of states of 4 s orbital of the zinc and 3p orbital of the sulphur [40]. The obtained band structure, total, partial and summed density of states indicates the semiconducting behaviour of ZnMgS NR thin film, which is in good agreement with the earlier theoretical reports obtained by DFT calculation through GGA and other approximation.

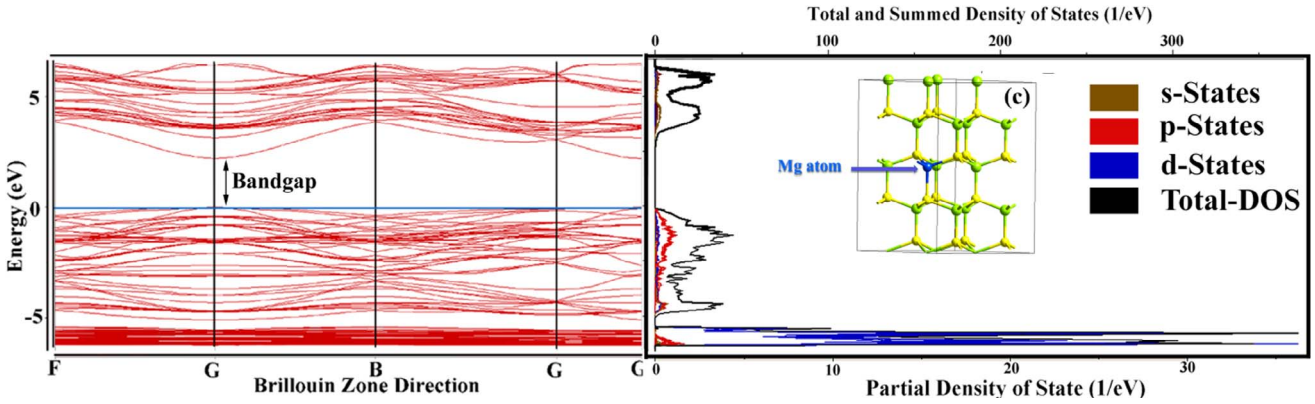

Fig. 6. (a) Band structure and (b) Density of states of ZnMgS.

4. Conclusion

ZnMgS NR was successfully grown by single-step chemical approach on to the glass substrate with a very short deposition time of 60 min and much lower bath temperature i.e. 65 °C. The reason for the choice of this growth method is that it is economically cheapest and easy to handle. The theoretical calculations revealed that ZnMgS shows the direct band semiconducting behaviour. These results have been correlated with the experimental results. From XRD analysis, nanocrystalline ZnMgS NR thin film revealed good crystallinity, the average crystallite size of ~23 nm along with this (0 0 2) peak intensity signifies the 1-D growth of NR's. Observation of estimated elemental composition in EDAX spectra confirms stoichiometry of the thin film. FESEM micrograph confirms the vertical growth of nanorods on the entire surface of the thin film. Also, ZnMgS NR thin film revealed higher absorbance in the UV region and energy bandgap of ~3.62 eV. The J-V graph shows increase in photocurrent when the light of 100Watt intensity is incident on samples. The features obtained in the experimental, as well as electronic structure of ZnMgS NR thin film, would be used for development of the next-generation optoelectronic application and photovoltaic devices.

Acknowledgements

A.S. Dive is thankful to UGC-DAE CSR Indore for the financial assistance (Ref. No. CSR-IC-BL-75/CRS-192/2016-17/856). We also thankful to Dr. F Singh, Sr. scientist IUAC New Delhi for a useful discussion.

References

[1] X.Q. Gu, L.P. Zhu, Z.Z. Ye, H.P. He, F. Liu, W. Jaeger, P.K. Chu, M.X. Qiu, Y.Z. Zhang, J.Y. Huang, Superlattices Microstruct. 44 (2008) 197–202.
[2] M.M. Fan, K.W. Liu, X. Chen, X. Wang, Z.Z. Zhang, B.H. Li, D.Z. Shen, ACS Appl. Mater. Interfaces 7 (2015) 20600–20606.
[3] K. Ichino, N. Suzuki, H. Kariya, K. Ueyama, M. Kitagawa, H. Kobayashi, J. Cryst. Growth 214 (2000) 368–372.
[4] I.K. Sou, M.C.W. Wu, K.S. Wong, G.K.L. Wong, J. Cryst. Growth 227 (2001) 705–709.
[5] G. Syrrokostas, K. Govatsi, S.N. Yannopoulos, Cryst. Growth Des. 16 (2016) 2140–2150.
[6] R. Yu, Q. Lin, S.-F. Leung, Z. Fan, Nano Energy 1 (2012) 57–72.
[7] X. Niu, S.P. Stagon, H. Huang, J.K. Baldwin, A. Misra, Phys. Rev. Lett. 110 (2013) 136102.
[8] A.S. Dive, N.P. Huse, K.P. Gattu, R. Sharma, AIP Conf. Proc. 1832 (2017) 120007.
[9] A. Kumar, K. Bhargava, T. Dixit, I.A. Palani, V. Singh, J. Electron. Mater. 45 (2016) 5606–5611.
[10] K. Gautam, I. Singh, P.K. Bhatnagar, K.R. Peta, Superlattices Microstruct. 93 (2016) 101–108.
[11] Y. Chen, R.-H. Yin, Q.-S. Wu, J. Nanomater. 2012 (2012) 1–6.
[12] P.K. Ghosh, U.N. Maiti, S. Jana, K.K. Chattopadhyay, Appl. Surf. Sci. 253 (2006) 1544–1550.
[13] A. Dehghan Banadaki, A. Kajbafvala, J. Nanomater. 2014 (2014) 1–28.
[14] I. Khan, I. Ahmad, H.A.R. Aliabad, M. Maqbool, J. Appl. Phys. 112 (2012).
[15] M. Wei, R.C. Boutwell, J.W. Mares, A. Scheurer, W.V. Schoenfeld, Appl. Phys. Lett. 98 (2011) 261913.
[16] Z.J. Othman, S. Ayed, A. Matoussi, H. Khemakhem, Vib. Spectrosc. (2016).
[17] Y.-H. Lai, W.-Y. Cheung, S.-K. Lok, G.K.L. Wong, S.-K. Ho, K.-W. Tam, I.-K. Sou, AIP Adv. 2 (2012) 012149.
[18] P. Kumar, J.P. Singh, Y. Kumar, A. Gaur, H.K. Malik, K. Asokan, Curr. Appl. Phys. 12 (2012) 1166–1172.
[19] C. Morhain, X. Tang, M. Teisseire-Doninelli, B. Lo, M. Laugt, J.M. Chauveau, B. Vinter, O. Tottereau, P. Vennegues, C. Deparis, G. Neu, Superlattices Microstruct. 38 (2005) 455–463.
[20] M.-H. Liang, Y.-T. Ho, W.-L. Wang, C.-Y. Peng, L. Chang, J. Cryst. Growth 310 (2008) 1847–1852.
[21] P. Chetri, B. Saikia, A. Choudhury, J. Appl. Phys. 113 (2013) 233514.
[22] P. Chetri, A. Choudhury, J. Alloys Compd. 627 (2015) 261–267.
[23] P. Chetri, B. Choudhury, A. Choudhury, J. Mater. Sci. (2014).
[24] O.F. Farhat, M.M. Halim, M.J. Abdullah, M.K.M. Ali, N.M. Ahmed, N.K. Allam, Appl. Phys. A 119 (2015) 1197–1201.
[25] K. Huang, Z. Tang, L. Zhang, J. Yu, J. Lv, X. Liu, F. Liu, Appl. Surf. Sci. 258 (2012) 3710–3713.
[26] N.P. Huse, A.S. Dive, K.P. Gattu, R. Sharma, Mater. Sci. Semicond. Process. 67 (2017) 62–68.
[27] R. Baghdad, N. Lemée, G. Lamura, A. Zeinert, N. Hadj-Zoubir, M. Bousmaha, M.A. Bezzerrouk, H. Bouyanfif, B. Allouche, K. Zellama, Superlattices Microstruct. 104 (2017) 553–569.
[28] I. Mohanty, C.K. Routray, U.P. Singh, Thin Solid Films 527 (2013) 147–150.
[29] V. Vasanthi, M. Kottaisamy, K. Anitha, V. Ramakrishnan, Superlattices Microstruct. 106 (2017) 174–183.
[30] A. Bedia, F.Z. Bedia, M. Aillerie, N. Maloufi, Superlattices Microstruct. (2017).
[31] D.J. Desale, S. Shaikh, A. Ghosh, R. Birajadar, F. Siddiqui, A. Ghule, R.B. Sharma, Composites Part B 43 (2012) 1095–1100.
[32] Z. Chen, X.X. Li, N. Chen, G. Du, Y. Li, G. Liu, A.Y.M. Suen, Mater. Sci. Eng. B 177 (2012) 337–340.
[33] N. Kılınç, L. Arda, S. Öztürk, Z.Z. Öztürk, Cryst. Res. Technol. 45 (2010) 529–538.
[34] B.S. Mwankemwa, M.J. Legodi, M. Mlambo, J.M. Nel, M. Diale, Superlattices Microstruct. 107 (2017) 163–171.
[35] I. Khan, A. Afaq, H.A. Rahnamaye Aliabad, I. Ahmad, Comput. Mater. Sci 61 (2012) 278–282.
[36] A. Djelal, K. Chaibi, N. Tari, K. Zitouni, A. Kadri, Superlattices Microstruct. (2017).
[37] N. Ullah, G. Murtaza, R. Khenata, J. Rehman, H. Ud Din, S. Bin Omran, Mater. Sci. Semicond. Process. 26 (2014) 681–689.
[38] Z.-Q. Yu, Z.-M. Xu, X.-H. Wu, Chin. Phys. B 23 (2014) 107102.
[39] F.C. Zhang, H.W. Cui, X.X. Ruan, W.H. Zhang, Appl. Mech. Mater. 556–562 (2014) 177–180.
[40] C. Feigl, S.P. Russo, A.S. Barnard, Mol. Simul. 37 (2011) 321–333.